Biosensors and Bioelectronics xx (xxxx) xxxx–xxxx

Contents lists available at ScienceDirect

Biosensors and Bioelectronics

journal homepage: www.elsevier.com/locate/bios

Target-triggered DNA nanoassembly on quantum dots and DNAzyme-modulated double quenching for ultrasensitive microRNA biosensing

Rui Yuan[a,b,1], Xiaolin Yu[b,1], Yuhong Zhang[a], Lulu Xu[a,b], Wei Cheng[a,*], Zhiguang Tu[b], Shijia Ding[b]

[a] The Center for Clinical Molecular Medical detection, The First Affiliated Hospital of Chongqing Medical University, Chongqing 400016, PR China
[b] Key Laboratory of Clinical Laboratory Diagnostics (Ministry of Education), College of Laboratory Medicine, Chongqing Medical University, Chongqing 400016, PR China

ARTICLE INFO

Keywords:
Quantum Dots
DNA nanoassembly
DNAzyme
Fluorescence quenching
MicroRNA

ABSTRACT

Herein, a simple and novel fluorescence biosensing strategy has been developed for ultrasensitive determination of microRNA (miRNA) by combining target-triggered DNA nanoassembly on quantum dots (QDs) with DNAzyme-modulated double quenching of QDs. In presence of miRNA target, the target triggered catalytic hairpin assembly (CHA) amplification and powered highly efficient DNA nanoassembly on the surface of QDs, leading to exhibition of numerous G-quadruplexes close to the QDs. The G-quadruplex folded properly and bound hemin to form a stable G-quadruplex/hemin complex. Then the luminescence of QDs was quenched via photoinduced electron transfer by hemin associated with the particles and the electron acceptor of O_2 which was in situ generated with the horseradish peroxidase-mimicked G-quadruplex/hemin DNAzymes toward H_2O_2. Based on this target-triggered highly efficient DNA nanoassembly and DNAzyme-modulated double quenching mechanism, the proposed biosensing strategy showed admirable signal amplification capability. Using miRNA-21 as model analyte, the designed nanosensor could detect miRNA down to 37 fM with a wide linear detection range of 1×10^{-13} M to 1.0×10^{-8} M, and exhibited good selectivity, acceptable reproducibility and low matrix effect. This proposed strategy presented a simple, powerful platform toward ultrasensitive miRNA detection and had great potential for bioanalysis and clinic diagnostic application.

1. Introduction

Semiconductor quantum dots (QDs) have become powerful tools for biological imaging, sensing and diagnostics because of their unique optical property and the nanometric dimensions (Zunger, 1998; Redl et al., 2003). Different QDs-based biosensor was developed with the rising in various analytic platforms, such as electrochemiluminescence (ECL) (Wu et al., 2016), chemiluminescence (CL) (Lee et al., 2016), electrochemical (Liu et al., 2015), surface plasmon resonance (SPR) and other platforms (Ghrera et al., 2016; Wang et al., 2016). Especially, the QDs are regarded as promising luminescence nano-probe in fluorescence biosensing (Benayas et al., 2015; Jou et al., 2015), due to their advantages of size-tunable emission, broad absorption, narrow and symmetric photoluminescence spectra, strong luminescence, and robust photostability (Chinen et al., 2015; Wegner and Hildebrandt, 2015).

These QD-based fluorescence biosensing strategies commonly employed the mechanisms of photoinduced transfer of electronic energy and electrons between QDs and connected molecular partners to obtain especial luminescence signal in the analysis of biological interactions and recognizations (Silvi et al., 2015). Organic dyes have been applied in a number of these approaches as conventional fluorescent probes for the Förster resonance energy transfer of QDs (Geißler et al., 2016). However, the inherent drawbacks of organic dyes, such as poor photostability, easy photobleaching, small stokes shifts and short lifetimes, limited the high efficiency biosensing (Qian et al., 2014). More recently, the nanomaterials, such as gold nanoparticle and graphene oxide, have been demonstrated effective quenching of QDs and used as quenching probes for biosensing (Dyadyusha et al., 2005; Qian et al., 2014). However, the multiple bioconjugation of nanomaterials may lead to increased preparation complexity, insufficient reproducibility, storability and functionality (Geißler et al., 2016). Thus, extensive effort is still an urgent demand to improve the simplicity and efficiency of QD-based fluorescence biosensors.

Hemin (Fe (III)-protoporphyrin IX) as the catalytic center of peroxidase, myoglobin and hemoglobin could conjugate to G-quad-

* Corresponding author.
E-mail address: chengwei@hospital.cqmu.edu.cn (W. Cheng).
[1] These authors contributed equally to this work.

http://dx.doi.org/10.1016/j.bios.2016.11.002
Received 11 August 2016; Received in revised form 28 October 2016; Accepted 2 November 2016
Available online xxxx
0956-5663/

ruplex, a single-stranded guanine-rich nucleic acid, to form DNAzyme with peroxidase-mimicking activity (Travascio et al., 1998; Sharon et al., 2010). Compared with native enzyme of horseradish peroxidase, the catalytic activity of DNAzyme is slightly lower (Miranda-Castro et al., 2010). However, due to its easy synthesis, convenient store, and easy to assemble as a molecule for signal readout, G-quadruplex/hemin has attracted substantial recent research interest as an amplifying mimic bioenzyme labels for biosensing applications (Gill et al., 2008; He et al., 2006; Jin et al., 2010; Zhao et al., 2015). As interesting paradigm for the development of novel and simple QDs-based optical biosensing mechanism, G-quadruplex/hemin has been conjugated to QDs and implemented as electron/energy transfer probes pairing with QDs. Willner's group has used G-quadruplex/hemin DNAzyme to catalyze chemiluminescence, in the presence of H_2O_2/luminol, develop chemiluminescence resonance energy transfer (CRET)-based QD biosensing methods (Freeman et al., 2011; Liu et al., 2011). Also, the hemin center of this DNAzyme was found to act as an electron transfer acceptor to quench the luminescence of QDs (Sharon et al., 2010). This system could be applied to construct simple nanosensor for the detection of DNA or aptamer-substrate complexes without additional labels of dyes or nanomaterials (Liu et al., 2014; Zhang et al., 2013). Unfortunately, simplex quenching mechanism of photoinduced electron transfer (PET) of QDs with hemin resulted in relatively low sensitivity of these biosensors.

Aiming at exploring more highly efficient mechanism for QDs quenching and further improving the analytical performance of QD-based fluorescence biosensor, a simple and ultrasensitive microRNA (miRNA) biosensing strategy has been developed by integrating target-triggered DNA nanoassembly on QDs with G-quadruplex/hemin DNAzyme-modulated double quenching. In this biosensing system, the oligonucleotide capture probes (CP) was capped on CdTe/CdS/ZnS Core-shell QDs to anchor the DNA nanostructure on its surface. The miRNA targets could trigger catalytic hairpin assembly (CHA) amplification and powered highly efficient DNA nanoassembly on the surface of QDs, resulting in exposure of numerous G-quadruplexes near the QDs. The G-quadruplex folded properly and bound hemin to form a stable G-quadruplex/hemin DNAzyme. Then the luminescence of QDs was double quenched via PET with not only hemin close to the particles but also the in situ-generated O_2 catalyzed by the horseradish peroxidase-mimicked DNAzymes toward H_2O_2. Based on this target-triggered DNA nanoassembly and DNAzyme-modulated double quenching mechanism, the proposed biosensing strategy showed remarkable signal amplification capability.

MiRNA-21, as an attractive biomarker for tumor diagnostics, plays an important role in the courses of cell proliferation, cell invasiveness, angiogenesis (Kumarswamy et al., 2011; Zhang et al., 2011) and is significantly upregulated expression in different kinds of solid tumors. Therefore, this work used it as a model target miRNA to verify the practicability of the designed strategy. The proposed method showed a very high sensitivity and low matrix effect, presenting a simple and pragmatic platform toward ultrasensitive miRNA detection.

2. Materials and methods

2.1. Materials and reagents

Water solution CdTe/CdS/ZnS Core-shell QDs with carboxylic acid group were purchased from Beida Jubang Science & Technology Co., Ltd. (Beijing, China). Hemin and 1-(3-Dimethylaminopropyl)-3-ethylcarbodiimide hydrochloride (EDC) were obtained from Sigma-Aldrich (St. Louis, USA). Gold-view, DL500 DNA Marker and MiRNA-21 were got from TaKaRa (Dalian, China). TRIzol Reagent was procured from Invitrogen (Carlsbad, USA). All DNA oligonucleotides were synthesized by Sangon Biotechnology Co., Ltd. (Shanghai, China) and purified using high-performance liquid chromatography. The detailed oligonucleotide sequences are listed in Table S1. In order to prevent the target miRNA from degrading by the RNase in the system, all other reagents were of analytical grade and solutions were prepared and diluted by RNase-free water.

2.2. Apparatus

The fluorescence spectra were obtained by using a Cary Eclipse Fluorescence Spectrophotometer (Agilent Technologies, Palo Alto, CA). The UV–vis absorption spectrum was recorded with an UV-2550 UV–Visible spectrophotometer (Shimadzu, Kyoto, Japan). The gel electrophoresis was performed on the DYY-6C electrophoresis analyzer (Liuyi Instrument Company, China) and imaged on Bio-rad ChemDoc XRS (Bio-Rad, USA).

2.3. Preparation of CP-capped QDs

An amount of 2.5 nmol of CdTe/CdS/ZnS QDs solution was mixed with 3 mg of EDC to activate the carboxylic acid group on the surface of QDs, followed by the addition of 7.5 nmol of amido modified CP for conjugation of QDs and CP (Yuan et al., 2012). After incubation for 3 h at room temperature (RT) under shaking and free of light, the resulting sample was ultrafiltrated using Vivaspin concentrator (Sartorius, 10,000 MW) at 4000 g for 5 min at 4 °C to remove the non-conjugated CP. The obtained conjugates were ultrafiltrated with 1×PBS twice to obtain CP-capped QDs which was kept at 4 °C prior to use.

2.4. Assay protocol for target detection

40 μL target miRNAs with various concentration was added to a 120 μL reaction mixture containing 125 nM hairpin probe 1 (H1), 125 nM hairpin probe 2 (H2), about 1 μM prepared CP-capped QDs in TNaK buffer (20 mM pH 7.5 Tris–HCl, 125 mM NaCl, 20 mM KCl), and incubated at 37 °C for 30 min. Then, 40 μL of 0.5 μM freshly prepared hemin solution in HEPES buffer was added and reacted at RT for 30 min to form G-quadruplex/hemin DNAzymes on the QDs surface. Hereafter, after 1 μL aliquot of 0.5 μM H_2O_2 was added for 5 min, the fluorescence spectra were recorded from 460 nm to 700 nm with the excitation wavelength of 450 nm. The silt widths of excitation and emission were both 5 nm and the voltage was 700 v.

In the real sample detection, total RNA from MCF-7 human breast cancer cells lines was extracted with TRIzol Reagent, dissolved in RNase-free water and quantitated by A_{260} measurement (Chomczynski et al., 1995).

2.5. Gel electrophoresis

A 2% agarose gel electrophoresis analysis of the products via the CHA reaction was carried out in 1× TBE buffer (90 mM Tris–HCl, 90 mM boric acid, 2 mM EDTA, pH 7.9) at 120 mV for about 40 min

3. Results and discussion

3.1. Design of the miRNA biosensing strategy

An overview of the designed fluorescence biosensing strategy for ultrasensitive MiRNA-21 detection was illustrated in Fig. 1. This target detection protocol included three serial reactions: target-triggered DNA nanoassembly on QDs, formation of G-quadruplex/hemin DNAzyme and DNAzyme-modulated double quenching. In the DNA nanoassembly step, H1 was designed to bind the target and initiate mismatched CHA amplification, which contained four parts including the target recognition region, CP hybridization region, H2 toehold region and G-quadruplex sequence. Once H1 specifically recognized and bound with the target, its hairpin opened and exposed the CP hybridization region and H2 toehold region, and deprotected the caged G-quadruplex sequence. Then H1-H2-CP DNA nanostructure was

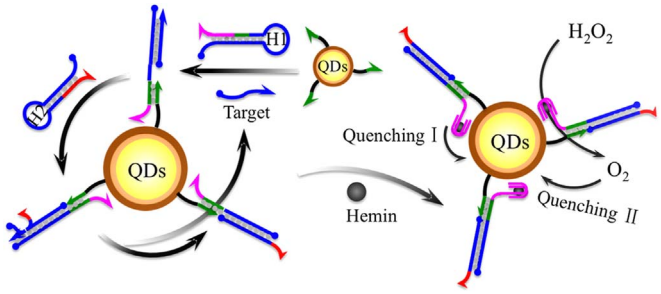

Fig. 1. Schematic representation of the ultrasensitive miRNA biosensing based on target-triggered DNA nanoassembly on QDs and DNAzyme-modulated double quenching.

assembled on the QDs surface via anchoring H1 on the CP-capped QD and toehold-induced strand displacement of target with H2. The released target could cyclically bind with other H1 probes and trigger new nanoassembly, leading to presentation of lot of G-quadruplexes on the QDs surface, which significantly amplified the target recognition event and facilitated the subsequent double quenching of QDs.

The presented G-quadruplexes subsequently bound with hemin to form G-quadruplex/hemin DNAzyme which played double roles to remarkably quench the luminescence of QDs as follows: (i) photo-excited electrons could be transferred to the Fe^{III} center of hemin (Zhang et al., 2013); (ii) G-quadruplex/hemin DNAzyme also acted as horseradish peroxidase to catalyze the H_2O_2 for in situ producing the electron acceptor of O_2, leading to a further quench of QDs fluorescence. (Zhao et al., 2015; Zang et al., 2014). Based on this target-triggered highly efficient DNA nanoassembly and DNAzyme-modulated double quenching mechanism, the proposed biosensing strategy could implement ultrasensitive quantitation of target miRNA.

3.2. Feasibility of the target-triggered DNA nanoassembly on QD surface

The synthesized process of the CP-capped QDs was based on the covalent binding of amido and carboxylic acid group. The average diameter of CdTe/CdS/ZnS QDs was about 4 nm, which was characterized by transmission electron microscopic image (Fig. S1). Water solution CdTe/CdS/ZnS QDs and the obtained CP-capped QDs were then characterized by absorption and emission spectra (Fig. 2A). The appearance of a new absorption peak at 260 nm indicated the successful biofunctionalization of QDs with the CP. The decrease in fluorescence intensity after biofunctionalization step indicated the decrease in the quantum yield, which was attributed to additional surface defects upon the association of the oligonucleotides.

To validation the process of the CHA, different reaction products were characterized by agarose gel electrophoresis. As shown in Fig. 2B, when H1 was hybridized with target miRNA, the product exhibited one dispersive band with relative less migration than that of H1, which represented a well integration of the target and H1 (lane 5). After H2 was added in this system, a more centralized band with slightly slower migration was obtained, indicating the production of multiple H1-H2 complexes via cyclical toehold-induced strand displacement of target with H2 (lane 7). These results proved the feasibility of the CHA process directly (Yan et al., 2015). In addition, the reaction products of H1/H2 and target/H2 did not display visible added bands (lane 3, 6), further confirming a high specificity of the designed CHA.

Previously, researcher preferred to directly modify the hairpin probes with QDs to conjugate the G-quadruplex to QDs (Sharon et al., 2010; Hao et al., 2015). Herein, short chain CP capped on QDs was used to integrate with CHA for DNA nanoassembly on QDs surface. As shown in Fig. 2C, compared with the control test by using hairpin probe H1-capped QDs directly, the CP-capped QDs showed higher luminescence signal responding to blank (curve a) and significantly lower signal responding to 10 nM of target miRNA (curve b), resulting in 8 times quenching ratio as much as that of H1-capped QDs. The result induced higher efficiency and specificity of CP-mediated DNA nanoassembly. Presumably, because it did not need to fold hairpin on QDs surface and had less steric hindrance for the DNA assembly reaction.

An imperfect CHA without H2, which only assembled target-H1 on QDs, was used as control to further prove the amplification of CHA for high efficiency of DNA nanoassembly on QDs surface (Fig. 2D). Compared with the control test, the method with complete CHA responding to 10 nM miRNA showed approximately 3 times lower fluorescence signal, illustrating the designed CHA significantly amplified the target recognition event indeed.

3.3. Verification of DNAzyme-modulated double quenching

After target-triggered DNA nanoassembly on QD surface, different means of quenching was investigated to testify the DNAzyme-modulated double quenching (Fig. 3C). When only hemin was in the quenching system, there was about 20% of quenching ratio responding to 10 nM target miRNA (curve b), owing to simplex PET from the QDs to the hemin bound with the G-quadruplexes on QDs surface. Meanwhile, H_2O_2 in the system really resulted in a nonspecific fluorescence quenching of the luminescence of the QDs (curve c). But the nonspecific influence of the hemin and H_2O_2 on the quenching system could be excluded by designing blank control (curve d) and using quenching ratio as readout signal for quantitative analysis. The quenching ratio was defined as $(F_B-F_S)/F_B$. F_B and F_S are the obtained fluoresence intensity responding to blank and samples, respectively. When hemin and H_2O_2 participate in the system simultaneously, the fluorescence emission signal was quenched for about 70% (curve e). The remarkable quenching attributed to the further PET form DQs to the electron acceptor of O_2 which was in situ generated with the high horseradish peroxidase-mimicked catalytic capacity of G-quadruplex/hemin DNAzymes toward H_2O_2, which play more significant role in the double quenching system (Lin et al., 2011). Besides, the designed control groups proved that this double quenching of the QDs originated from the specific organization of the G-quadruplex/hemin structure on the QDs surface, rather than from a nonspecific binding of hemin to the oligonucleotides-capped QDs or free hemin in the system (Fig. 3A, B). These results strongly confirmed the feasibility, high efficiency and specificity of G-quadruplex/hemin DNAzyme-modulated double quenching mechanism.

3.4. Optimization of CP-Capped QDs

In order to achieve high signal amplification of the DNA nanoassembly and double quenching, several important experimental parameters were investigated. The coverage of the CP on the QDs surface had a great influence on the DNA nanoassembly efficiency and fluorescence quenching. As shown in Fig. 4A, 3 times of CP to QDs achieved the maximum quenching ratio. Lower ratio of CP to QDs resulted in lower fluorescence quenching due to insufficient sites for binding H1-H2 complexes on QDs. On the other hand, the excessive CP probes on the QDs surface could increase the steric hindrance, leading to lower efficiency of DNA nanoassembly. Thus, 1:3 of CP to QDs was selected as the optimum reaction ratio for preparation of CP-Capped QDs, which is consistent with the 3 times of amplification efficiency of CHA-based nanoassembly (Fig. 2D), and indicating that the maximum number of G-quadruplexes to QDs was estimate to be 3 times.

PET effect was highly sensitive to the distance between the QDs and the G-quadruplex/hemin complex (Sharon et al., 2010; Zhang et al., 2013). In our work, the exposed G-rich DNA sequence in HI-H2-CP complex need sufficient space to flexibly fold into a G-quadruplexs tructure and bind with hemin near QDs surface. So, an olig(T)-linker was designed in the 5' end of CP to control the distance between the

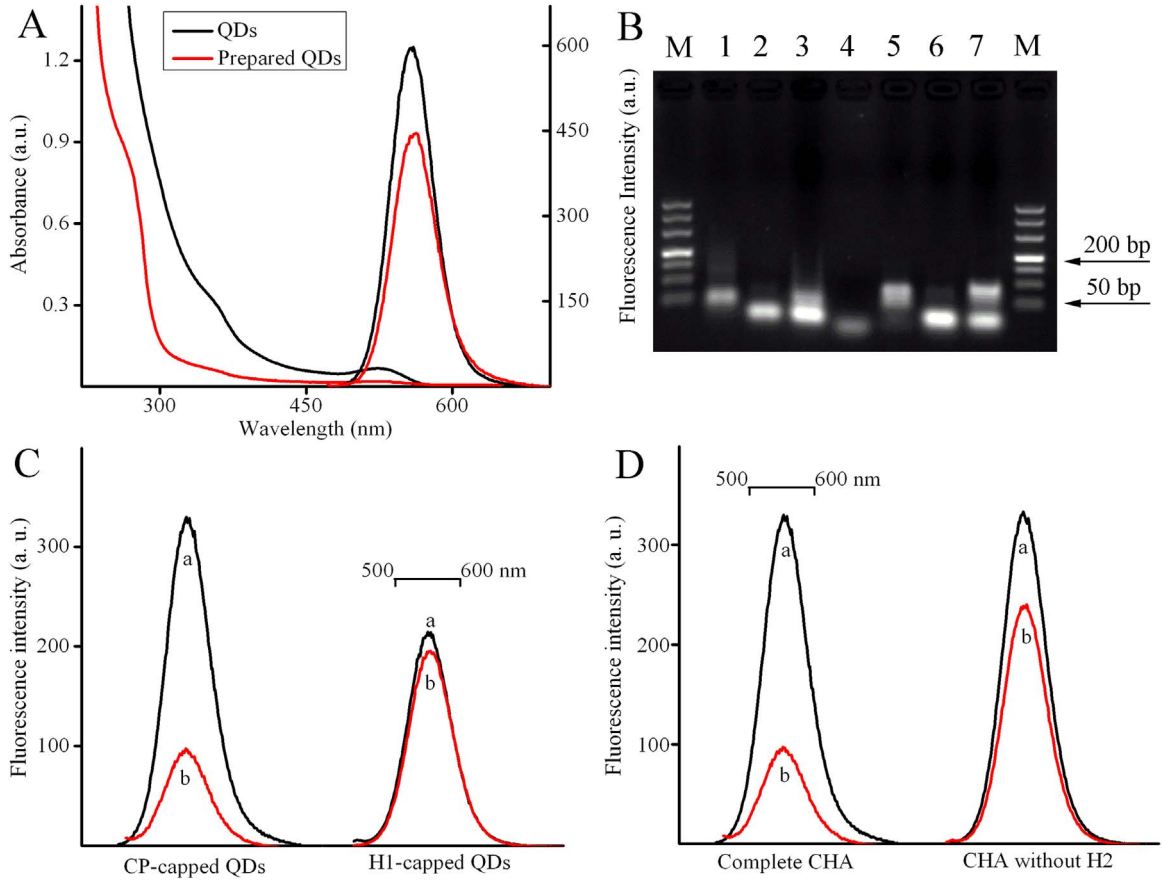

Fig. 2. (A) Absorption and emission spectra of water solution CdTe/CdS/ZnS Core-shell QDs and prepared CP-capped QDs. (B) Gel electrophoresis analysis of H1 (lane 1), H2 (lane 2), H1 and H2 (lane 3), MiRNA-21 (lane 4), reaction products of MiRNA-21 with H1 (lane 5), MiRNA-21 with H2 (lane 6), and MiRNA-21 with H1 and H2 (lane 7). (C) Fluorescence emission spectra of the CP-capped and H1-capped QDs responding to blank (a) and 10 nM MiRNA-21 (b), respectively. (D) Fluorescence emission spectra of the designed biosensor with completed CHA and imperfect CHA without H2 in responding to blank (a) and 10 nM MiRNA-21 (b), respectively.

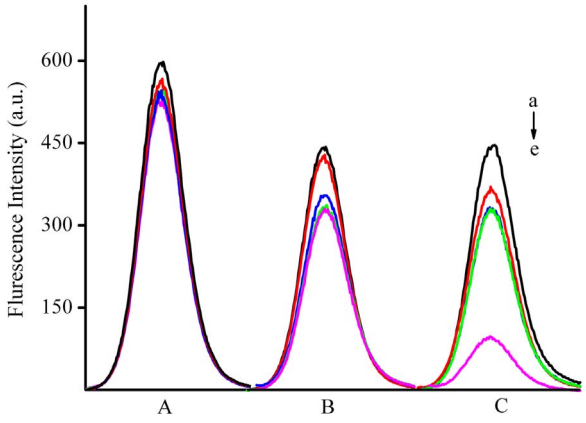

Fig. 3. Typical fluorescence emission spectra of (A) unmodified QDs, (B) unmatched CP-capped QDs and (C) CP-capped QDs responding to 10 nM target using the quenching system without hemin and H_2O_2 (a), with 100 nM of hemin (b), 0.5 μM of H_2O_2 (c), 100 nM of hemin and 0.5 μM of H_2O_2 (e), and responding to blank with 100 nM of hemin and 0.5 μM of H_2O_2 (d), respectively.

QDs and the G-quadruplex (Table S1). As shown in Fig. 4B, with the increasing base numbers of olig(T)-linker, the obtained quenching efficiency increased and then tended to reach the maximum value at 10 bases. Then, increasing base numbers led to rapidly decreased quenching efficiency, due to the increased distance separating the G-quadruplex/hemin from the QDs. Therefore, 10 bases of olig(T) were chosen as the best linker of CP for assembling the G-quadruplex contained DNA nanostructure on QDs.

3.5. Optimization of conditions for double quenching

The concentrations of H_2O_2 and hemin in the system had a great influence on the quenching ratio. With the increasing concentration of H_2O_2, the fluorescence signals responding to blank and 10 nM miRNA target simultaneously decreased and the quenching ratio tended to a maximum value at 0.5 μM of H_2O_2 (Fig. 5A, B). Thereafter, the quenching ratio decreased with the increasing H_2O_2 due to increased nonspecific fluorescence quenching. Similarly, the maximum quenching ratio was indeed achieved at 100 nM of hemin responding to 10 nM target miRNA (Fig. 5C, D). Thus, 0.5 μM of H_2O_2 and 100 nM of hemin were selected as the optimal conditions for double fluorescence quenching.

3.6. Analytical performance of biosensor

Under the optimal experimental conditions, the fluorescence intensity responses gradually decreased with the elevated concentration of the target MiRNA-21 (Table S2 and Fig. 6A). The plot of the luminescence quenching ratio vs. the logarithm of target MiRNA-21 concentration showed a strong linear relationship in the range from 10 nM to 100 fM with a correlation coefficient of 0.998 (Fig. 6B). The limit of the detection (LOD) was calculated to be 37 ± 0.92 fM (n=3). For comparison, we also investigated the analytical property of the method using simplex quenching of QDs with hemin. As shown in Fig. 6C and D, this assay was carried out from 10 nM to 100 pM with the LOD of 11 ± 1.26 pM (n=3). The LOD of our designed biosensor based on target-triggered DNA nanoassembly and DNAzyme-modulated double quenching was approximately 3 orders of magnitude lower

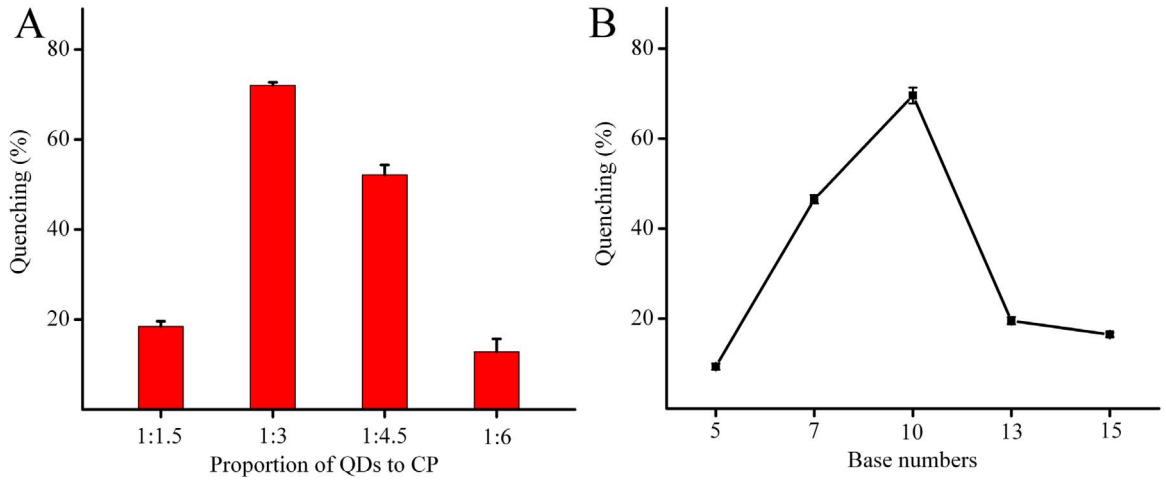

Fig. 4. Dependences of luminescence quenching ratio on (A) the concentration ratio of QDs to CP for the CP-capped QDs preparation, (B) the base number of olig(T)-linker in CP near QDs surface, respectively. Error bars are standard derivation obtained from three independent experiments.

than that of the control method and reported biosensors using hemin quenching alone (Sharon et al., 2010; Zhang et al., 2013). Meanwhile, the proposed method also had a superior sensitivity than that of mismatched CHA based biosensor (Zhang et al., 2015) and those assays with enzyme-assisted signal amplification, such as exonuclease III-assisted CHA, rolling circle replication and so on (Peng et al., 2014; Xu et al., 2014) (Table S3). More importantly, such a performance was obtained within about 1 h of total detection time without additional labeling, enzymic catalysis and complicated analysis operation.

To estimate the reproducibility of the developed biosensing strategy, the intra-assay imprecision of five different detections at one assay and inter-assay imprecision at five different batch QDs for MiRNA-21 detection were examined, respectively. The intra-assay coefficient of variation (CV) was 4.15% and the inter-assay CV was 12.77%. Thus the

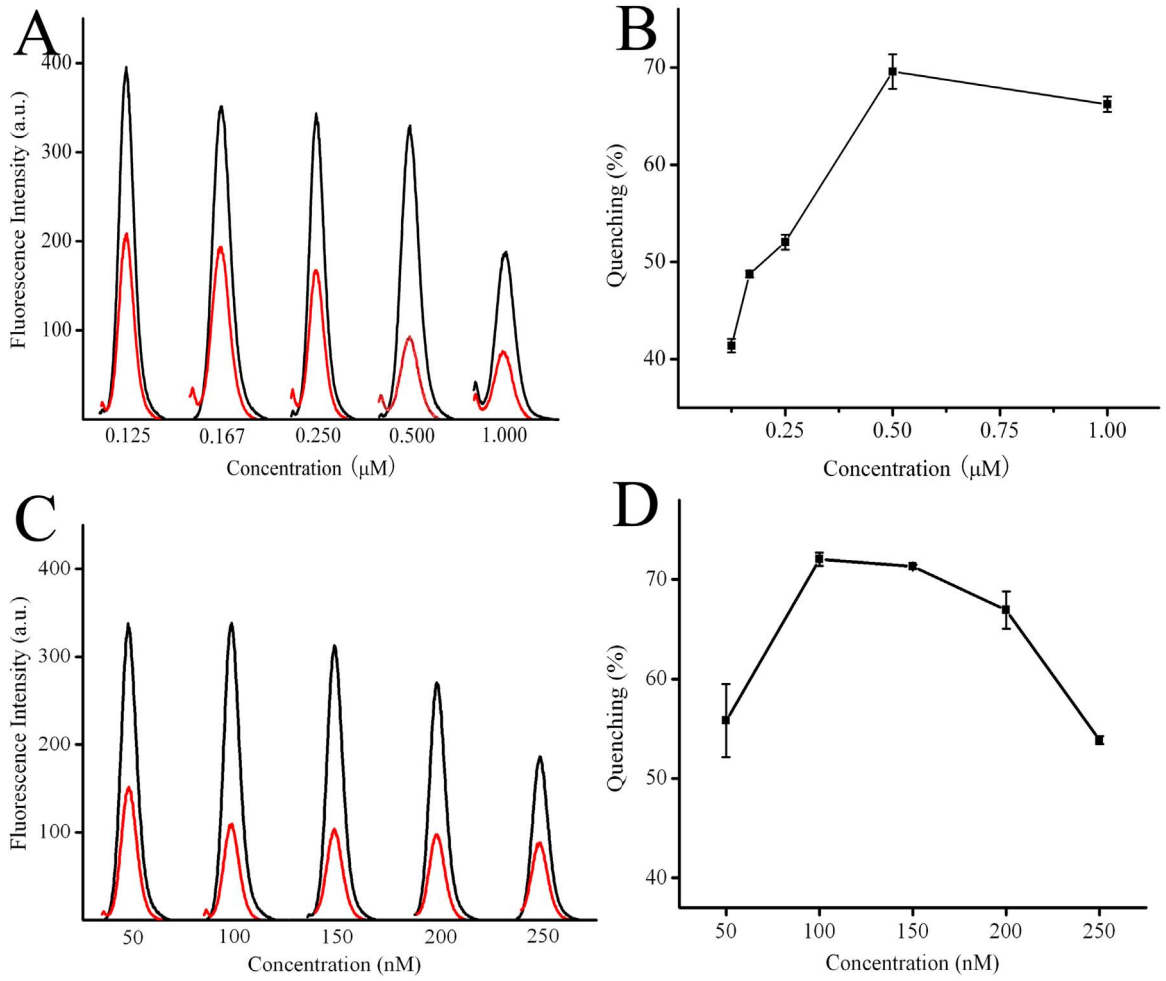

Fig. 5. Dependences of luminescence spectra responding to blank (black) and 10 nM target (red), and its luminescence quenching ratio on the different concentration of H_2O_2 (A, B) and hemin (C, D), respectively.

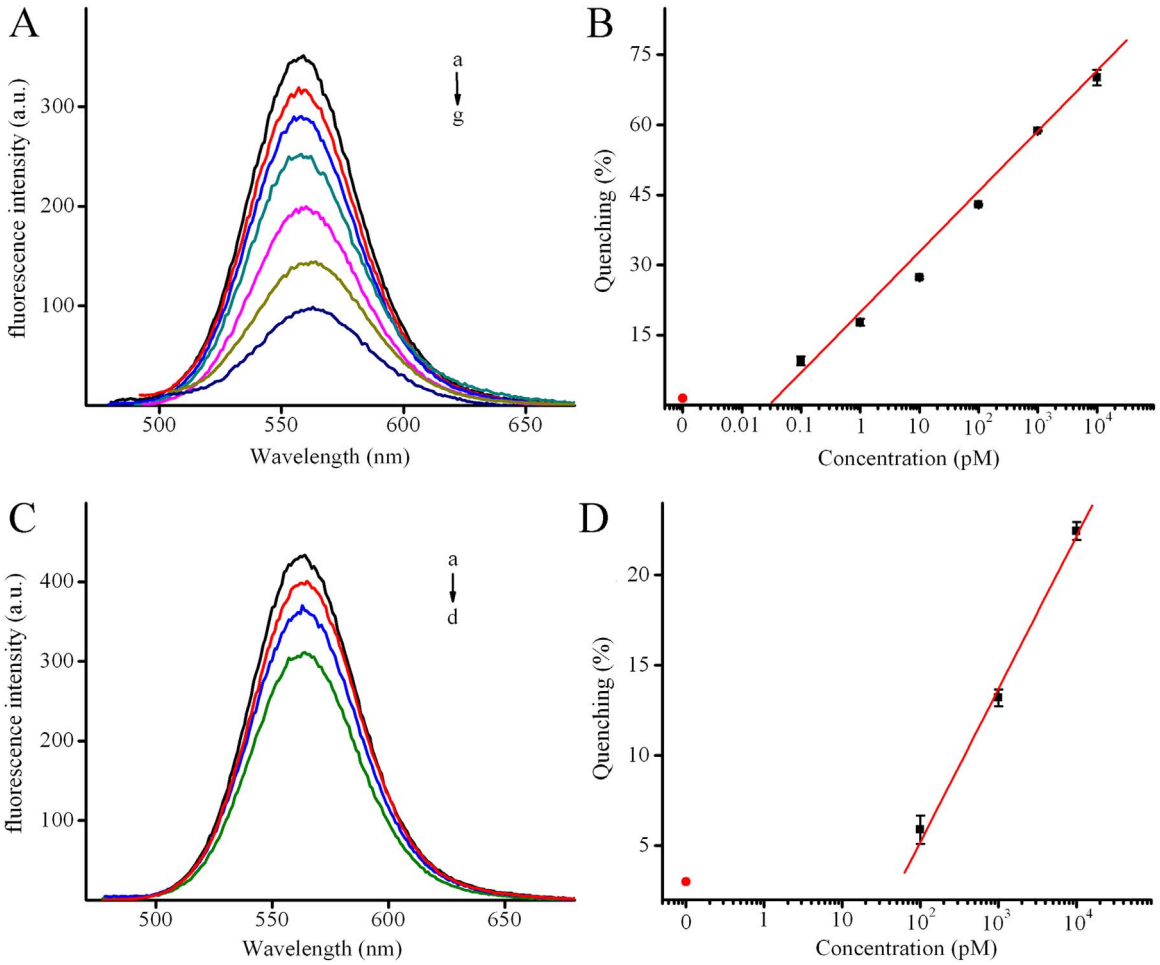

Fig. 6. (A) Luminescence spectra and (B) calibration curve of the proposed biosensor responding to 0, 0.1, 1, 10, 100 pM and 1, 10 nM of the target MiRNA-21 (from a to g). (C) Luminescence spectra and (D) calibration curve of the control bisoensor with only 100 nM hemin in the quenching system responding to 0, 100 pM and 1, 10 nM of the target MiRNA-21 (from a to d), respectively. Error bars are standard derivation obtained from three independent experiments.

precision and reproducibility of the proposed biosensing strategy was acceptable.

3.7. Real sample analysis

To further evaluate the analytical reliability and application potential, the proposed method was used to analysis MiRNA-21 in total RNA extracted from MCF-7 human breast cancer cell line. The total RNA was diluted to 870 ng μL^{-1} and used for detection. The amount of MiRNA-21 in 870 ng of total RNA sample was estimated to be about 66 amol (165 fM in 400 μL of reaction solution) (RSD=1.1%, n=5), according to the calibration curve (Fig. 6B). To further evaluate its performance in real sample analysis, different amounts of MiRNA-21 were spiked into 870 ng total RNA for the assay. The results showed the recovery of 109–112%, suggesting that the method have a low matrix effect, and great potential for sensitively detect miRNA in real sample (Table S4).

4. Conclusion

In summary, the present study has demonstrated a simple and ultrasensitive fluorescence biosensor for convenient detection of miRNA based on target-triggered DNA nanoassembly on QDs surface and DNAzyme-modulated double quenching of QDs. The target-triggered DNA nanoassembly showed high signal amplification capability and the DNAzyme-modulated double quenching mechanism proved high specificity and efficiency for quenching of QDs. The designed method thus showed an ultra-high sensitivity, acceptable reproducibility and low matrix effect. Furthermore, such an excellent analysis performance was obtained within about 1 h of total detection time without additional labeling, enzymic amplification and complicated analysis operation This proposed strategy presents a simple and pragmatic platform toward ultrasensitive miRNA detection and shows great potential for clinic diagnostic application.

Acknowledgements

This work was funded by the National Natural Science Foundation of China (81572080), the Natural Science Foundation Project of Chongqing (cstc2015shmszx120086 and cstc2014kjrc-qnrc10001), the Science Foundation Projects of Chongqing Municipal Education Commission (KJ1500218) and Yuzhong District of Chongqing (20150114), the Research Innovation Project for Post Graduate of Chongqing Municipal (CYS15118).

Appendix A. Supplementary material

Supplementary data associated with this article can be found in the online version at doi:10.1016/j.bios.2016.11.002.

References

Benayas, A., Ren, F., Carrasco, E., Marzal, V., del Rosal, B., Gonfa, B.A., Juarranz, A., Sanz-Rodríguez, F., Jaque, D., García- Solé, J., Ma, D., Vetrone, F., 2015. Adv. Funct. Mater. 25, 6650–6659.

Chinen, A.B., Guan, C.M., Ferrer, J.R., Barnaby, S.N., Merkel, T.J., Mirkin, C.A., 2015. Chem. Rev. 115, 10530–10574.
Chomczynski, P., Mackey, K., 1995. Biotechniques 19, 942–945.
Dyadyusha, L., Yin, H., Jaiswal, S., Brown, T., Baumberg, J.J., Booy, F.P., Melvin, T., 2005. Chem. Commun. 25, 3201–3203.
Freeman, R., Liu, X.Q., Winner, I., 2011. J. Am. Chem. Soc. 133, 11597–11604.
Geißler, D., Hildebrandt, N., 2016. Anal. Bioanal. Chem. 408, 4475–4483.
Ghrera, A.S., Pandey, M.K., Malhotra, B.D., 2016. Biosens. Bioelectron. 80, 477–482.
Gill, R., Bahshi, L., Freeman, R., Willner, I., 2008. Angew. Chem. Int. Ed. 120, 1700–1703.
Hao, N., Dai, P.P., Yu, T., Xu, J.J., Chen, H.Y., 2015. Chem. Commun. 51, 13504–13507.
He, F., Tang, Y., Yu, M., Wang, S., Li, Y., Zhu, D., 2006. Adv. Funct. Mater. 16, 91–94.
Jin, H., Heller, D.A., Kalbacova, M., Kim, J.H., Zhang, J., Boghossian, A.A., Maheshri, N., Strano, M.S., 2010. Nat. Nanotechnol. 5, 302–309.
Jou, A.F.J., Lu, C.H., Ou, Y.C., Wang, S.S., Hsu, S.L., Willner, I., Ho, J.A.A., 2015. Chem. Sci. 6, 659–665.
Kumarswamy, R., Volkmann, I., Thum, T., 2011. RNA Biol. 8, 706–713.
Lee, E.S., Deepagan, V.G., You, D.G., Jeon, J., Yi, G.R., Lee, J.Y., Lee, D.S., Suh, Y.D., Park, J.H., 2016. Chem. Commun. 52, 4132–4135.
Lin, D., Wu, J., Yan, F., Deng, S.Y., Ju, H.X., 2011. Anal. Chem. 83, 5214–5221.
Liu, H., Lou, Y., Zhou, F., Zhu, H., Abdel-Halim, E.S., Zhu, J.J., 2015. Biosens. Bioelectron. 71, 249–255.
Liu, S.Y., Na, W.D., Pang, S., Su, X.G., 2014. Biosens. Bioelectron. 58, 17–21.
Liu, X.Q., Freeman, R., Golub, E., Willner, I., 2011. ACS Nano 5, 7648–7655.
Miranda-Castro, R., Lobo-Castañón, M.J., Miranda-Ordieres, A.J., Tuñón-Blanco, P., 2010. Electroanalysis 22, 1297–1305.
Peng, Y., Jiang, J., Yu, R., 2014. Anal. Methods 6, 2889–2893.
Qian, Z.S., Shan, X.Y., Chai, L.J., Ma, J.J., Chen, J.R., Feng, H., 2014. Nanoscale 6, 5671–5674.
Redl, F.X., Cho, K.S., Murray, C.B., O'Brien, S., 2003. Nature 42, 968–971.
Sharon, E., Freeman, R., Willner, I., 2010. Anal. Chem. 82, 7073–7077.
Silvi, S., Credi, A., 2015. Chem. Soc. Rev. 44, 4275–4289.
Travascio, P., Li, Y., Sen, D., 1998. Chem. Boil 5, 505–517.
Wang, Y., Wu, B., Yang, C., Liu, M., Sum, T.C., Yong, K.T., 2016. Small 12, 534–546.
Wegner, K.D., Hildebrandt, N., 2015. Chem. Soc. Rev. 44, 4792–4834.
Wu, P., Hou, X., Xu, J.J., Chen, H.Y., 2016. Nanoscale 8, 8427–8442.
Xu, F.Z., Shi, H., He, X.X., Wang, K., He, D.G., Guo, Q.P., Qing, Z.H., Yan, L.A., Ye, X.S., Li, D., Tang, J.L., 2014. Anal. Chem. 86, 6976–6982.
Yan, Y.R., Shen, B., Wang, H., Sun, X., Cheng, W., Zhao, H., Ju, H.X., Ding, S.J., 2015. Analyst 140, 5469–5474.
Yuan, L., Xu, L.L., Liu, S.Q., 2012. Anal. Chem. 84, 10737–10744.
Zang, Y., Lei, J.P., Zhang, L., Ju, H.X., 2014. Anal. Chem. 86, 12362–12368.
Zhang, H.L., Yang, L.F., Zhu, Y., Yao, X.D., Zhang, S.L., Dai, B., Zhu, Y.P., Shen, Y.J., Shi, G.H., Ye, D.W., 2011. Prostate 71, 326–331.
Zhang, L.B., Zhu, J.B., Guo, S.J., Li, T., Li, J., Wang, E., 2013. J. Am. Chem. Soc. 135, 2403–2406.
Zhang, Y., Yan, Y.R., Chen, W.H., Cheng, W., Li, S.Q., Ding, X.J., Li, D.D., Wang, H., Ju, H.X., Ding, S.J., 2015. Biosens. Bioelectron. 68, 343–349.
Zhao, M., Liao, N., Zhuo, Y., Chai, Y.Q., Wang, J.P., Yuan, R., 2015. Anal. Chem. 87, 7602–7609.
Zunger, A., 1998. MRS Bull. 23, 15–17.